

High-Yield Chemical Synthesis of Hexagonal ZnO Nanoparticles and Nanorods with Excellent Optical Properties

P. K. Giri^{1,2,*}, S. Bhattacharyya¹, B. Chetia³, Satchi Kumari¹, Dilip K. Singh², and P. K. Iyer³

¹Department of Physics and ²Centre for Nanotechnology, Indian Institute of Technology, Guwahati 781039, India

³Department of Chemistry, Indian Institute of Technology, Guwahati 781039, India

Large yield and low temperature growth of nanostructures are key requirements for fulfilling the demand of large scale applications of nanomaterials. Here, we report a highly efficient chemical method to synthesize high quality hexagonal ZnO nanoparticle and nanorods utilizing the low temperature oxidation of metallic zinc powder in the presence of an appropriate catalyst. This one-step method has advantages such as low temperature (90 °C) and atmospheric pressure synthesis and a high yield (>90%). Microstructure and optical properties of the as-synthesized ZnO nanoparticles are found to be identical or better than those of the commercial ZnO nanopowder (Sigma-Aldrich). In particular, in comparison to the commercial nanopowder the as-grown ZnO nanorods and nanoparticles exhibit stronger UV absorption at 376 nm and intense UV photoluminescence emission at ~382 nm, with negligible defect emission band. This method is suitable for large-scale production of nanosized ZnO and could be extended for the synthesis of other metal oxides.

Keywords: ZnO Nanostructures, High-Yield Chemical Synthesis, HRTEM, Photoluminescence, Raman.

1. INTRODUCTION

Large yield and controlled synthesis of nanostructures are key components for the manufacturing of nanodevices. For nanomaterials, achieving higher purity and crystalline structure are important for studying their physical and chemical properties. Nanostructured ZnO materials have drawn broad attention due to its wide range of applications in ultraviolet (UV) lasers,¹ power generators,² solar cells,³ gas sensors,⁴ field emission devices,⁵ capacitors, varistors, transparent UV resistance coating, photoprinting, electrophotography, electrochemical and electromechanical nanodevices, sun screen lotion (cream), cosmetic and medicated creams etc.^{6–9} Some of the future applications include catalysts for organic reactions and delivering drugs to infected areas of body.

Many synthetic methodologies for zero- and one-dimensional ZnO nanostructures have been developed,^{10–12} including vapor phase methods¹³ and aqueous methods.¹⁴ The vapor-phase method usually employs vacuum, sophisticated equipment and elevated temperature which restrict the type of substrate used, in contrast to the low-cost and

simple aqueous methods. However, simple methods for preparation of high quality nanostructures with high yield and good control on shape and size are very less. Among the aqueous methods, the hydrothermal method¹⁵ has emerged as a powerful method for the fabrication of one-dimensional nanomaterials with some significant advantages, such as controllable structures and a cost-effective, low-temperature, substrate independent and less-complicated technique. However, yield and quality of the product material is usually not addressed. For example, Kale et al.¹⁶ reported synthesis of high-yield of flower-like ZnO nanorods using a hydrothermal method. However, near band edge UV emission was not observed from those samples due to poor quality of the material and large defect concentration. Similarly, large-scale synthesis of ZnO flower-like and brush pen-like nanostructures by a hydrothermal decomposition route showed very weak UV emission and strong green emission.¹⁷ In majority of the studies, the product suffers from poor optical properties due to presence of large concentration of intrinsic defects in ZnO. Chu et al recently reported a solution-based, high-yield synthesis of cobalt-doped ZnO nanorods with room temperature ferromagnetism.¹⁸ Xu et al. reported on the high-yield synthesis of single-crystalline ZnO hexagonal

*Author to whom correspondence should be addressed.

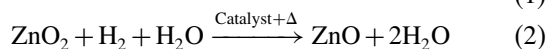
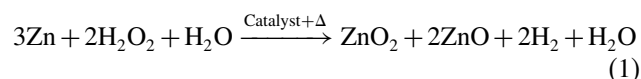
nanoplates.¹⁹ However, the reported studies have product yield below 50%. Hence, large scale and high yield synthesis of defect free ZnO nanostructures is imperative to meet the demand for emerging applications.

In this paper, we report a simple, low cost, low temperature method with high yields (>90%) of synthesizing ZnO nanostructures using two different catalysts. Depending on the catalyst and reaction conditions, different shapes such as nanorods, nanoneedles, hexagonal nanoparticles (NPs), nanoflower-like structures are obtained. The as-synthesized ZnO nanostructures were characterized using X-ray diffraction (XRD), Scanning electron microscope (SEM), UV-visible absorption, photoluminescence (PL) and Raman spectra. The results are compared with those of the commercially available ZnO nanopowders (Sigma Aldrich, mean particle size 50–70 nm).

2. EXPERIMENTAL DETAILS

2.1. Synthesis of ZnO Nanostructures

All chemicals with high purity were used as purchased from Merck and Sigma Aldrich. In a typical reaction, 1.2 g of Zn powder was added to a round bottom flask fitted with a reflux condenser. Water and 30% H₂O₂ solution were added to this flask which was stirred continuously at 90 °C for 5 hrs. Water to H₂O₂ ratio was 1:1 (v/v) for all the reactions. Two different catalysts, namely acetic acid (Catalyst A) and trifluoroacetic acid (catalyst B) were used for these reactions and either of the two was added to the reaction mixture after few minutes of starting the reaction. White colored precipitates were formed in the reaction solution indicating the formation of ZnO, which were separated by centrifuge and subsequently washed with distilled water. The powder formed was dried in vacuum. It was observed that all the reactions yielded 90–95% yield and the reaction could be scaled to much higher quantities without appreciable loss in the final product. The reaction pathway leading to high yield ZnO product could be as follows:



We have found that at 90 °C during the initial stage of reaction, primarily ZnO₂ is formed along with ZnO, and the ZnO₂ later converts to ZnO for longer duration reaction. In such as growth, one can expect a ZnO core with thin ZnO₂ shell even for sufficient reaction time. The catalyst plays an important role in deciding the morphology of the NPs. We find that at a fixed temperature of reaction, use of acetic acid yields preferably hexagonal ZnO NPs, and trifluoroacetic acid induces the growth of ZnO nanorods. With the increase of reaction time, the quality of the ZnO nanopowder improves. We find that size of the

NPs or nanorods do not depend on the initial size of the Zn particles used for reaction. Similar product was also found using Zn nanopowders as starting material. For convenience of discussion, the sample prepared with catalyst A for 5 1/2 hrs of reaction is named as ZnO33, the sample prepared with catalyst B for 6 hrs of reaction is referred as ZnO32 and the commercial ZnO nanopowder is referred as ZnO_nano.

2.2. Microstructure and Optical Characterization

The as-grown ZnO NPs were then characterized using a powder X-ray diffraction (XRD) system (Seifert 3003 T/T), scanning electron microscope (SEM) and Transmission electron microscopy (TEM). SEM measurements were performed using Model LEO 1430VP for studying the morphology of nanoparticles. Energy dispersive X-ray (EDX) analysis was performed using the same SEM apparatus. High resolution (HR) TEM measurements were carried out with 200 keV electrons (2010 UHR JEOL). Optical properties of the powders were studied using UV-visible absorption, photoluminescence and Raman measurements. UV-visible absorption spectra were taken using a commercial spectrophotometer (Shimadzu 3101 PC). Photoluminescence spectra were obtained at room temperature using He-Cd laser (325 nm) as an excitation source and Jobin-Yvon T64000 spectrometer equipped with a cooled charged coupled detector. Raman spectra were recorded in the backscattering geometry using vertically polarized 488 nm Ar⁺ laser beam, double grating monochromator and cooled photo multiplier tube.

3. RESULTS AND DISCUSSION

3.1. Structure and Morphology

XRD pattern of ZnO33 and ZnO32 grown with catalyst A and B, respectively are shown in Figure 1. For comparison, XRD pattern of commercially procured ZnO nanopowder is also shown in the same figure. The patterns show distinct peaks related to the hexagonal structure of the ZnO, and a very low intensity peak (marked with arrow) corresponding to ZnO₂. Line widths of the ZnO related peaks are almost identical in these three samples. High intensity and narrow line width of the spectra are indicative of the good crystallinity of the NPs. Depending on the growth time and reaction temperature, the crystallinity of the product varies. It is found that crystallite size grows with increasing reaction time at an appropriate temperature. High quality of ZnO nanopowder was obtained after 6 hours of reaction with catalyst B at 90 °C. XRD analysis reveals that besides the ZnO peaks, intensity of the ZnO₂ peak is significant for the product obtained with shorter duration (1 1/2 hr to 3 hrs) of reaction. With increasing reaction time, intensity of ZnO peak grows gradually at a cost of decrease of ZnO₂ peak, and after 6 hrs of reaction

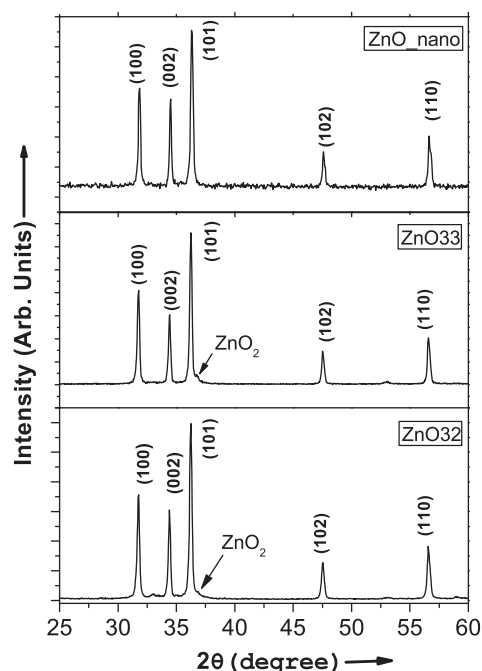


Fig. 1. XRD pattern of the as-synthesized ZnO nanostructures in ZnO32 and ZnO33, prepared with catalyst A and catalyst B, respectively. For comparison, XRD pattern for ZnO_nano is also shown.

crystalline ZnO peak is very strong, with negligible content of ZnO₂. As the ZnO NPs size grows with reaction time, the line width of the XRD pattern decreases with increasing reaction time. Ignoring the effect of anisotropic

strain on the XRD line shape broadening and using Scherrer formula we estimate average size of ZnO crystallites as ~50 nm after 4 hours of reaction and ~90 nm after 6 hrs reaction. XRD line profile shows that the sample obtained after 1/2 hr of reaction has average crystallite (ZnO) size <10 nm.

The morphology of the nanostructures obtained after 4 hours of reaction was studied using SEM. The SEM images as shown in Figures 2(a)–(c) exhibit varieties of typical shapes obtained in this method, such as, hexagonal NPs, nanorods, nanoneedles and nanoflowers, depending on the catalysts and reaction time. For comparison, morphology of commercial ZnO nanopowders is shown in Figure 2(d). EDX spectra taken on all four samples show higher fraction of oxygen content in the product due to presence of ZnO₂ shell over ZnO core NPs and a proper stoichiometry of Zinc and oxygen is obtained after 6 hours of reaction. The higher oxygen content is due to the presence of ZnO₂ in the product formed with 4 hrs of reaction.

Figure 3 shows HRTEM images of the samples prepared with catalyst A after 4 hrs of reaction. Initial stage of the growth can be understood from Figure 4(a) where small crystallites of ZnO are shown with dotted oval regions that act as nucleation site for further growth of NCs. Figure 3(b) shows a relatively large ZnO NP, where one face of the hexagonal structure is truncated, indicating an incomplete growth of the NP. Inset shows the corresponding selected area electron diffraction

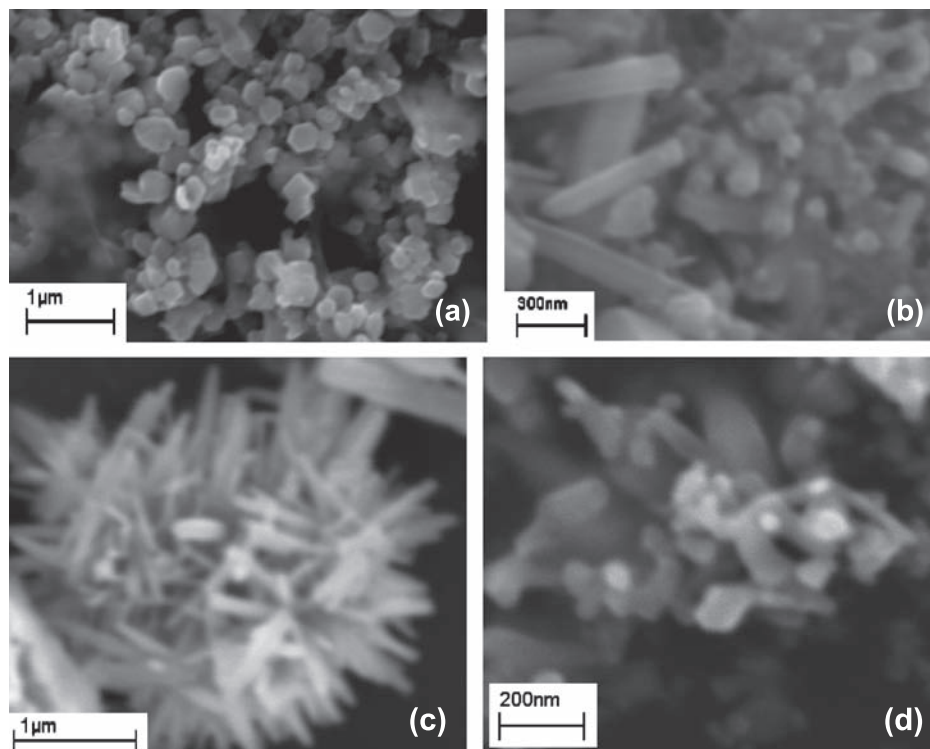


Fig. 2. SEM images of ZnO NPs obtained after 4 hrs of reaction: (a) with catalyst A showing hexagonal NPs, (b) with catalyst B showing hexagonal nanorods, (c) with catalyst B showing nanoflower like bundling of nanorods; (d) commercial ZnO nanopowder.

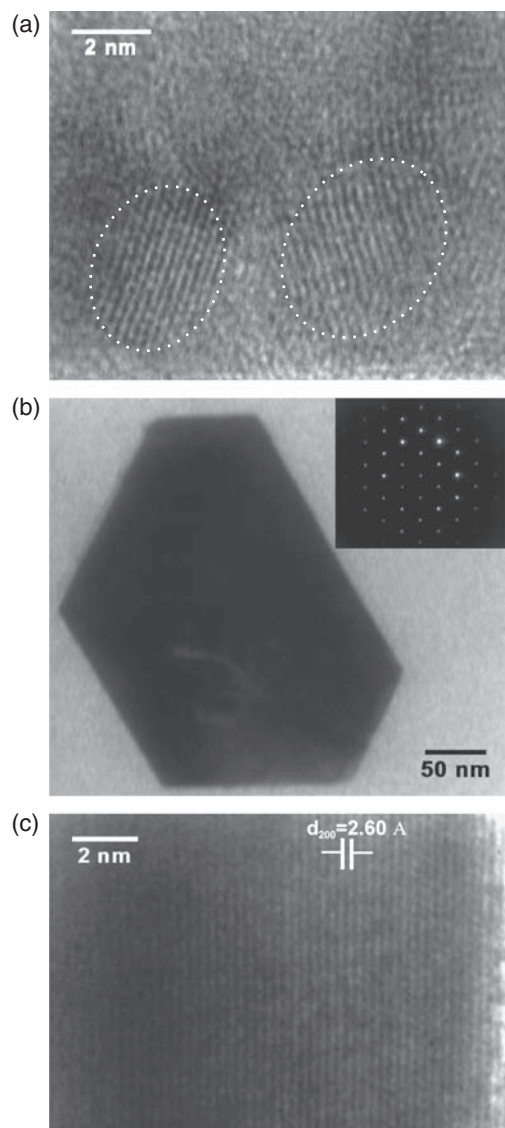


Fig. 3. HRTEM images of ZnO NPs grown after 4 hrs of reaction with catalyst A: (a) Small nanocrystal seed of ZnO, (b) hexagonal nanoparticle truncated at one edge and the corresponding SAED pattern, (c) high resolution lattice image of ZnO NP showing perfect crystalline structure.

(SAED) pattern confirming the crystallinity of the product. Figure 3(c) shows the high resolution lattice image of one such NP. The interplanar d -spacing calculated from the image matches closely with the (002) plane d -spacing of hexagonal ZnO.

HRTEM images of ZnO33 (5^{1/2} hrs reaction) is shown in Figure 4. Figure 4(a) shows the morphology of the hexagonal ZnO NPs and the corresponding SAED pattern indicating crystallinity of the product. The NP shape grows to perfectly hexagonal shape after in this sample, while a truncated hexagonal shape was obtained after 4 hrs of reaction. Figure 4(b) show a typical high resolution image of a nanorod in the same sample and the lattice image showing (002) planes of ZnO with d -spacing value as expected for perfect crystalline ZnO. A careful observation

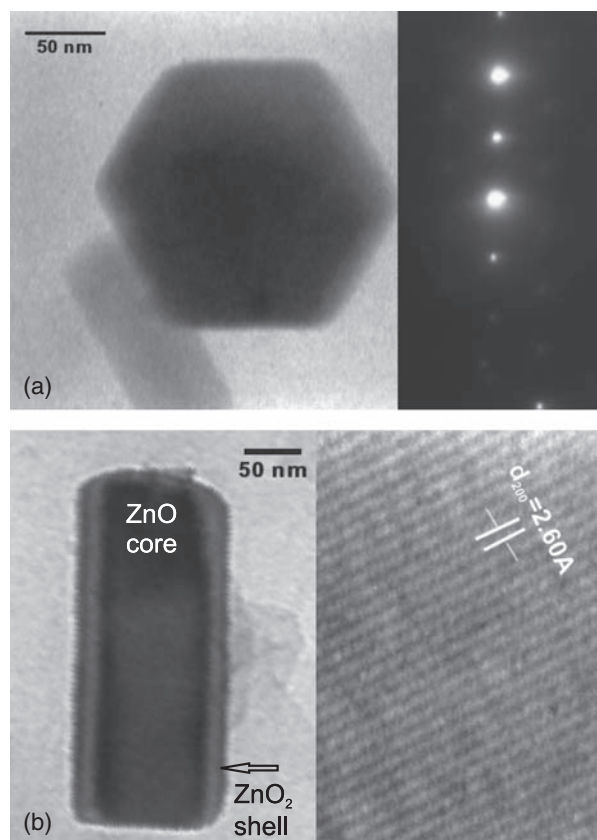


Fig. 4. HRTEM image of ZnO33 samples after 5 1/2 hrs of reaction: (a) perfect hexagonal shaped NP with corresponding SAED pattern, (b) a nanorod with crystalline ZnO core and ZnO₂ shell. The corresponding lattice image of the core region shows the lattice spacing of (002) planes of hexagonal ZnO.

of the nanorod shown in Figure 4(b) reveals the dark core region is surrounded by a relatively bright thin shell region. Thus the as-grown nanorods have a core–shell structure with crystalline ZnO in the core and a thin ZnO₂ shell region. This is consistent with the XRD pattern shown in Figure 1. Optical properties of such a core–shell structure are expected to be different from the one without a shell region.

3.2. Optical Properties

UV-Visible absorption spectra of the as-grown ZnO nanopowder and commercial nanopowder are shown in Figure 5. The room temperature spectra exhibit strong excitonic absorption peaks at ~ 378.2 nm and ~ 376.2 nm for samples ZnO33 and ZnO32, respectively. The position of the absorption peak closely matches with that of the commercial ZnO nanopowder. It is important to note that ZnO32 samples containing mostly ZnO nanorods show much higher UV absorption as compared to the commercial nanopowder. This is attributed to large surface area of the nanorods as compared to the irregular shaped NPs in ZnO_nano sample. This high absorbance of the

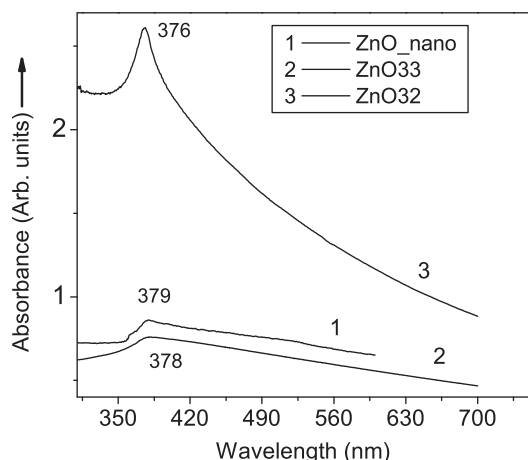


Fig. 5. Comparison of UV-visible absorption spectra for ZnO33, ZnO32 and ZnO_nano samples. ZnO32 shows much higher UV absorbance as compared to the ZnO_nano sample.

as-prepared ZnO nanorods has important implication for applications in optoelectronics and cosmetic industry.

Figure 6 shows the comparison of PL spectra for ZnO32, ZnO33 and ZnO_nano. The spectra features are almost identical for all three samples. Different constituents peaks

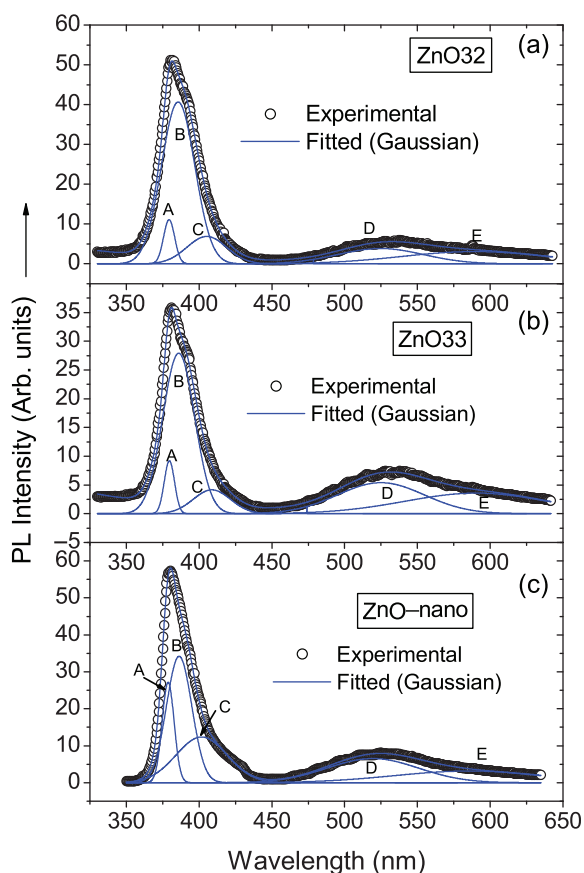


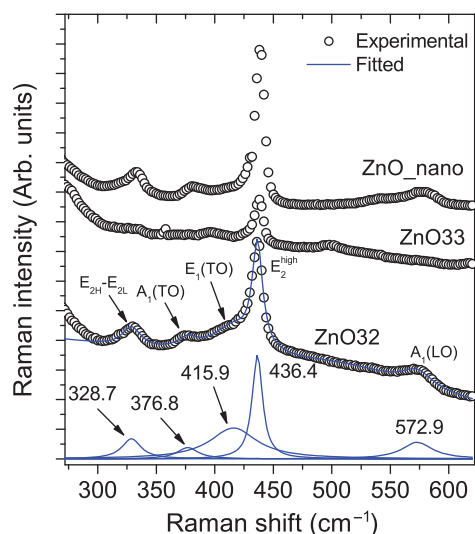
Fig. 6. Comparison of PL spectra for (a) ZnO32 and (b) ZnO33 with that of the (c) ZnO_nano sample. Experimental data are shown with symbols and fitted (Gaussian) peaks are shown with solid lines. Details of the fitted peak parameters are presented in Table I.

fitted with Gaussian line shape are shown as solid line. Details of the fitted peaks and possible identity of each peak is given in Table I. Peak positions and line widths of all five peaks are very similar in these samples. The ~ 380 nm emission originates from the recombination of free excitons through an exciton–exciton collision process corresponding to near band edge (NBE) emission of wide band gap ZnO.²⁰ This peak is the most important signature of the high quality of the product. The 390 nm peak is due to transition in the band-tail states of ZnO nanorods. These band-tail states are caused by the disorder/defects at the surface of the nanorods.^{21,22} Further, an inspection of the relative intensity of the UV and visible peaks reveals that ZnO nanorods have stronger band-edge emission than the ZnO NPs. The intensity of the green emission is less in ZnO32 as compared to both ZnO_nano and ZnO33 samples, indicating superior quality of the product obtained after 6 hrs of reaction with catalyst B. Thus, the nanorods obtained in our methods have superior UV absorption as well as UV emission properties as compared to the commercial ZnO nanopowder. The bands in the visible region are related to zinc vacancy and oxygen vacancies.^{23,24} The peak E at ~ 590 nm is related to surface defects/disorder of ZnO nanorods. The ZnO32 samples show very low intensity peak in the visible region and hence defect concentration is extremely low in this sample. Further improvement in optical properties can be made by thermal annealing of the as-prepared product. We find that sample prepared with 4 hrs of reaction shows strong visible PL emission (>500 nm) besides the expected strong UV emission from ZnO. The visible emission believed to be due to the presence of ZnO₂ and the surface defects in the nanorods. One may expect to suppress the visible emission by thermal annealing of the as-grown product.

Figure 7 show a comparison of the Raman spectra of commercial ZnO nanopowder and the as-grown ZnO nanorods and NPs. The spectra show several peaks characteristics of vibrational modes in ZnO single crystal. The peak positions and full width at half maxima (FWHM) are derived by the fitting Lorentzian line shapes to the spectra in each case. Peak at ~ 328 cm⁻¹ in Figure 6(b) is due to E_{2H}–E_{2L} mode. Peaks at 376.8 cm⁻¹ and 415.9 cm⁻¹ are due to well known A₁(TO) and E₁(TO) modes. The modes E₁(TO) and A₁(TO) reflect the strength of the polar lattice bonds. These two modes are relatively weak in ZnO33 sample. E₂^(high) mode at 436.4 cm⁻¹ is most prominent in these samples, similar to bulk ZnO. The E₂^(high) mode represents the band characteristic of wurtzite phase.²⁵ Peak position and FWHM are almost identical in these three samples including commercial ZnO nanopowders (Sigma Aldrich), suggesting again an excellent crystallinity of the samples. This is consistent with the HRTEM studies. Peak at 572.9 cm⁻¹ is related to A₁(LO) mode. In bulk ZnO, A₁(LO) mode at 578 cm⁻¹ has been attributed to oxygen vacancy or zinc interstitial or their complexes.²⁶

Table I. Summary of the fitted PL peaks shown in Figure 6. A Gaussian line shape is fitted for each peak.

Samples	Peak position in nm (FWHM in nm)				
	A	B	C	D	E
ZnO32	379.4 (8.9)	385.6 (27.0)	405 (32.1)	524.7 (69.4)	589.3 (116.7)
ZnO33	379.6 (8.3)	386.0 (25.8)	408.8 (30.1)	524.9 (70.3)	590.4 (114.9)
Zno_nano	378.7 (9.8)	386.3 (20.5)	401.7 (41.2)	519.3 (73.9)	585.8 (12.2)
Peak identify	Bound excitons	Band-tail states	V_{Zn}	O_{Zn}	Surface disorder

**Fig. 7.** Comparison of Raman spectra of ZnO32 and ZnO33 with ZnO_nano sample. Constituent peaks (center of the peak labeled in cm^{-1}) are fitted with Lorentzian line shape after background subtraction.

4. CONCLUSIONS

We have synthesized high quality hexagonal ZnO nanoparticles and nanorods by catalyst driven oxidation of metallic zinc at a low temperature and atmospheric pressure. This method yields greater than 90% of high purity product in the presence of any of the two catalysts. A ZnO/ZnO₂ core-shell structure is formed in products obtained with shorter duration of reaction. The optical properties of the as-prepared products are found to be superior to the commercial ZnO nanopowder. The XRD pattern shows excellent crystallinity of the product. The SEM and TEM images show hexagonal cross section of the NPs and nanorods. As-grown samples show strong UV absorption peak at ~ 378 nm. Room temperature PL spectra show strong UV emission peak at ~ 380 nm and negligible green emission, indicating good optical properties of the samples. Raman scattering studies confirmed high crystallinity of the ZnO nanostructures.

Acknowledgments: This work was partly supported by the financial assistance from UGC-DAE project and BRNS project. PKI thanks CSIR, New Delhi, India and DST, New Delhi, India for financial assistance. We thank

Dr. P. V. Satyam, Institute of Physics, Bhubaneswar for help in the HRTEM measurements.

References and Notes

- M. H. Huang, S. Mao, H. Feick, H. Yan, Y. Wu, H. Kind, E. Weber, R. Russo, and P. Yang, *Science* 292, 1897 (2001).
- X. Wang, J. Song, J. Liu, and Z. L. Wang, *Science* 316, 102 (2007).
- C. Y. Jiang, X. W. Sun, G. Q. Lo, D. L. Kwong, and J. X. Wang, *Appl. Phys. Lett.* 90, 263501 (2007).
- Q. Wan, Q. H. Li, Y. J. Chen, T. H. Wang, X. L. He, J. P. Li, and C. L. Lin, *Appl. Phys. Lett.* 84, 3654 (2004).
- C. Y. Lee, S. Y. Li, P. Lin, and T.-Y. Tseng, *IEEE Tran. Nanotechnol.* 5, 216 (2006).
- H. T. Wang, B. S. Kang, F. Ren, L. C. Tien, P. W. Sadik, D. P. Norton, S. J. Pearton, and J. Lin, *Appl. Phys. Lett.* 86, 243503 (2005).
- J. J. Wu, G. R. Chen, H. H. Yang, C. H. Ku, and J. Y. Lai, *Appl. Phys. Lett.* 90, 213109 (2007).
- S. F. Yu, Clement Yuen, S. P. Lau, W. I. Park, and G. C. Yi, *Appl. Phys. Lett.* 84, 3241 (2004).
- N. Serpone, D. Dondi, and A. Albini, *Inorganica Chimica Acta* 360, 794 (2007).
- Z. Fan and J. G. Lu, *J. Nanosci. Nanotechnol.* 5, 1561 (2005).
- Y. W. Heo, D. P. Norton, L. C. Tien, Y. Kwon, B. S. Kang, F. Ren, S. J. Pearton, and J. R. LaRoche, *Mater. Sci. Engg. R* 47, 1 (2004).
- G. C. Yi, C. Wang, and Won Il Park, *Semicond. Sci. Technol.* 20, S22 (2005).
- Z. L. Wang, *J. Phys.: Condens. Matter* 16, R829 (2004).
- L. Vayssieres, *Adv. Mater.* 15, 464 (2003).
- G. W. Ho and A. S. W. Wong, *Appl. Phys. A* 86, 457 (2007).
- R. B. Kale, Y. J. Hsua, Y. F. Lina, and S. Y. Lu, *Solid State Commun.* 142, 302 (2007).
- W. Bai, K. Yu, Q. Zhang, F. Xu, D. Peng, and Z. Zhu, *Mater. Lett.* 61, 3469 (2007).
- D. Chu, Y. Zeng, and D. Jiang, *J. Am. Ceramic Soc.* 90, 2269 (2007).
- F. Xu, Z.-Y. Yuan, G.-H. Du, M. Halasa, and B.-L. Su, *Appl. Phys. A* 86, 181 (2007).
- K. Thonke, Th. Gruber, N. Teofilov, R. Schonfelder, A. Waag, and R. Sauer, *Physica B* 308–310, 945 (2001).
- Q. P. Wang, D. H. Zhang, Z. Y. Xue, and X. T. Hao, *Appl. Surf. Sci.* 201, 123 (2002).
- F. Demangeot, V. Paillard, P. M. Chassaing, C. Pagès, M. L. Kahn, A. Maisonnat, and B. Chaudret, *Appl. Phys. Lett.* 88, 071921 (2006).
- B. Lin, Z. Fu, and Y. Jia, *Appl. Phys. Lett.* 79, 943 (2001).
- T. Moe Børseth, B. G. Svensson, A. Yu. Kuznetsov, P. Klason, Q. X. Zhao, and M. Willander, *Appl. Phys. Lett.* 89, 262112 (2006).
- Y. Yang, H. Yan, Z. Fu, B. Yang, L. Xia, Y. Xu, J. Zuo, and F. Li, *Solid State Commun.* 138, 521 (2006).
- R. Ayouchi, D. Leinen, F. Martin, M. Gabas, E. Dalchiele, and J. R. Ramos-Barrado, *Thin Solid Films* 426, 68 (2003).

Received: 15 February 2008. Accepted: 19 March 2009.